Synthesis Of Pb-based and Pb-free Perovskite Systems

Parth Raval
MS14137

A dissertation submitted for the partial fulfillment of BS-MS dual degree in Science

Indian Institute of Science Education and Research Mohali
April 2019

Certificate of Examination

This is to certify that the dissertation titled **"Synthesis Of Pb-based And Pb Free Perovskite Systems"** submitted by **Mr. Parth Raval** (Reg. No. MS14137) for the partial fulfillment of BS-MS dual degree programme of the Institute, has been examined by the thesis committee duly appointed by the Institute. The committee finds the work done by the candidate satisfactory and recommends that the report be accepted.

Dr. Ujjal K Gautam Dr. Subhabrata Maiti Dr.Debrina Jana
(Supervisor)

Dated: April 25, 2019

Declaration

The work presented in this dissertation has been carried out by me under the guidance of Dr. Debrina Jana at the Indian Institute of Science Education and Research Mohali.

This work has not been submitted in part or in full for a degree, a diploma, or a fellowship to any other university or institute. Whenever contributions of others are involved, every effort is made to indicate this clearly, with due acknowledgment of collaborative research and discussions. This thesis is a bonafide record of original work done by me and all sources listed within have been detailed in the bibliography.

Parth Raval

(Candidate)

Dated: April 25, 2019

In my capacity as the supervisor of the candidate's project work, I certify that the above statements by the candidate are true to the best of my knowledge.

Dr. Debrina Jana

(Supervisor)

Acknowledgment

I wish to express my deepest gratitude to my supervisor, Dr. Debrina Jana for inspiration, continued encouragement, valuable suggestions, and support during my 5th year at IISER. Her mentorship has helped me become a better scientific writer, strategic planner and critical thinker about science.

Additionally, I would like to thank Dr. Ujjal Gautam and Dr. Subhabrata Maiti for being members in my committee and for all kind suggestions related to my research.

I gratefully acknowledge DST INSPIRE faculty research grant (DST/INSPIRE/04/2015/002741) for funding this work and DST INSPIRE for the financial aid they provided in my scientific career.

I am thankful to Prof. Sanjay Mandal for helping us characterizing samples in XRD (central research facility, IISER Mohali). I would like to acknowledge INST for recording TEM images of my samples.

I would also like to thank and to express sincere appreciation to my coworkers, Isabella, Tinku, and Samita to provide a cooperative environment in the lab.

I am very thankful to Prabhat Singh Rana, Amreen Bains, Pinku Tung, Akanksha Jain, Shivam Mishra, Sheeba Khan, Vijay Gupta, Mayank Joshi, Debapriya Das and Dr. Swapnil for help they provided.

An acknowledgment with an excellent thanks goes to my friends, Nishant Naresh, Nilotpal Kakati, Shivangi Vaish, and Nitish Garg for always being my constant morale booster. It would have been a challenging journey without their continuous entertainment and encouragement.

Last but not least, I would like to thank my parents and my sister, Ami for unconditional love and inspirations that shaped my actions and morals.

Abbreviations

CB	Conduction Band
CIE	Commission Internationale De l'Elcairage
CPD	Carbon Polymer Dots
EDAX	Energy-Dispersive X-Ray Spectroscopy
FESEM	Field Emission Scanning Electron Microscopy
FTIR	Fourier-Transform Infrared Spectroscopy
FWHM	Full Width At Half Maximum
HRTEM	High-Resolution Transmission Electron Microscopy
LED	Light-Emitting Diode
NCs	Nanocrystals
PCE	Photoconversion Efficiency
PL	Photoluminescence
PSC	Perovskite Based Solar Cell
PV	Photovolataics
PXRD	Powder X-Ray Diffraction
QY	Quantum Yield
SAED	Selected Area Electron Diffraction
TCSPC	Time-Correlated Single Photon Counting
UV	Ultraviolet
VB	Valence Band

Contents

Abstract

Perovskite nanocrystals have emerged as a potential candidate in the field of optoelectronics specifically in next-generation backlit displays, LEDs, etc. Towards this goal, research is being carried out to synthesize stable perovskite NCs which can emit light entire the visible wavelength range. Here, in this thesis, we describe a protocol comprising perovskite NCs and Carbon quantum dots composite which emits white light upon UV light irradiation. Throughout the thesis, we have described the existing protocol in the literature, our approach and finally establishing the synthetic protocol to generate a white light emitting solution. Detailed characterizations including UV-vis, steady-state and time-resolved photoluminescence studies, XRD, electron microscopic characterizations were done to understand the processes involved therein.

In another attempt, we carried out research on antimony double perovskite-based systems in order to get rid of toxic and air and moisture sensitive Pb^{2+} based perovskites. This thesis describes two different approaches towards the synthetic protocol- solvent based synthesis and hot-injection method in order to obtain phase pure antimony based double perovskite materials. Optical, XRD and electron microscopic characterizations have been undertaken to realize the formation and property of these materials.

Chapter 1

Introduction

1.1 Perovskites

Most monovalent A^+ and divalent B^{2+} ions can form a complex halide with the stoichiometry ABX_3 (X = F, Cl, Br, I), which in turn often possess the perovskite structure.[1] The perovskite structure is generally described as a three-dimensional arrangement of a corner-sharing octahedral BX_6 unit,[2] with the A ion placed in the cuboctahedral interstices.

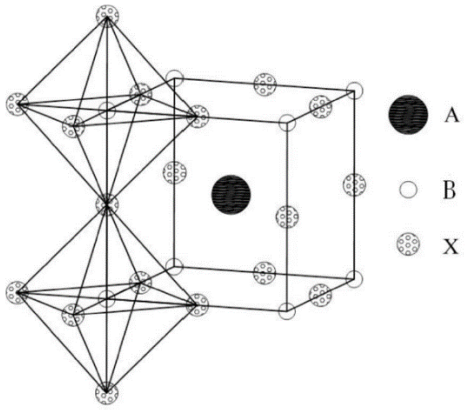

Figure 1: Cubic perovskite structure of ABX_3 (the figure has been reproduced from Ref.3) [3]

Perovskites are important crystal structures as they possess several sensational properties, such as a large optical transmission domain; high resistivity; antiferromagnetic; extraordinary magnetic; piezoelectric; photoluminescent properties; anionic conductivity over a wide temperature range. [4,5] Goldschmidt proposed tolerance factor which dictates the stability of ABX_3.[6] Up to now; almost all known perovskites have tolerance factor values in the range 0.75–1.00.

$$t = \frac{r_A + r_X}{\sqrt{2\,(r_B + r_X)}}$$

Where r_A, r_B, and r_X are the ionic radii for the ions in the A, B and X sites.

1.1.1 History

Colloidal semiconductor NCs (e.g., CdSe) are sub-20 nanometer semiconductor crystallites synthesized in the colloidal state wherein the molecular precursors are reacted at 25–400^{0}C using inexpensive solution-phase chemistry. Surface capping ligands are added to control the nucleation, growth, and long-term structural integrity. They have an electronic structure which is intermediate

between bulk solids and individual molecules. Control over composition, morphology, and self-assembly of colloidal NCs has induced a keen interest in colloidal semiconductors NCs and subsequently enabling applications in fields such as optoelectronics.[7]

The major challenge faced by semiconductor NCs has been to weaken the unfavorable electronic effects of their high surface area and under-coordinated surface sites which leads to the formation of trap states for charge carriers. As a consequence, semiconductor NCs are poorly luminescent in the visible spectral range. In parallel to work on colloidal semiconductor NCs, a significant discovery in perovskite NCs occurred in the form of methylammonium lead iodide ($MAPbI_3$) as an outstanding PV material[8] took place and has been the subject of intense research activity ever since leading to the demonstration of certified power conversion efficiencies in working PV cells of up to 23.3%.[9]

Utilization of MA-based compounds is not the best choice due to its inherently low chemical stability which ultimately leads to the formation of volatile decomposition products. It would drastically detriment the properties of perovskite and hence fully inorganic analogues based on cesium ($CsPbX_3$) are focused.

1.1.2 Synthesis and optical properties of cesium lead halide perovskite NCs

Unlike oxidic perovskites, lead halide perovskites are rather soft materials with comparatively low boiling points in the range of 300-570^{0}C. It has significant ionic bonding character, and hence its synthesis gets a bit easier. It can be represented as the arrested co-precipitation of ion sin apolar solvent in the presence of long chain capping ligands.[10] Cs-oleate is quickly injected into a hot solution of lead halide dissolved in octadecene containing capping ligands such as oleyl amine and oleic acid. An alternative synthetic strategy relies on the fast destabilization of molecular solutions; the lead halide source and cesium halide source is first dissolved in a ‘good’ solvent (highly polar) and then injected into a ‘poor’ solvent (non-polar) containing same capping ligands. Irrespective of the method of their preparation, Lead halide perovskite exhibit a bright PL spanning the entire visible spectral range.

Lead halide perovskites are direct bandgap semiconductors, and the states near the Valence Band (VB) and Conduction Band (CB) arise solely from the X and Pb atoms whereas the A-site ion has no substantial contribution into it. The VB is mainly formed via the hybridization of Pb 6s and halide 6p orbitals which results in the antibonding states whereas the conduction band is formed primarily of empty Pb 6p states. High ionic character reflects the low contribution of halide orbitals to the conduction band.

1.1.3 Defect tolerance in lead halide perovskites

It is well established that even with the extensive presence of defects, the photophysical properties of lead halide perovskites are not affected. This high tolerance for defects arises from the fact that the defects reside in relatively shallow states within the bandgap.[11] For instance, in $CsPbBr_3$, under Br-rich conditions, a vacancy on the Cs site has the lowest of all possible formation energy of 0.2eV. However, Cs orbitals do not contribute to the near band edge electronic structure, and hence Cs vacancy does not threat the PL properties of $CsPbBr_3$. Moreover, vacancies on the halide sites are also benign to its electronic properties since the corresponding nonbonding Pb orbital are resonant with the conduction band and the valence band.

1.1.4 The utilization of perovskites as white light emitting materials

White light emitting single compounds have always been given particular interest in optoelectronics since issues related to self-absorption and color instability that is caused by the presence of multi emitters can be avoided. Dohner and collaborators reported 2D hybrid perovskite as novel white-emitting material.[12] They used organic cation N-methylethane- 1,3-diammonium (N-MEDA) at A site. It showed broad emission with a peak maximum at 558nm with FWHM of 165nm. CIE color coordinate they obtained from this is 0.36/0.41. They also synthesized mixed halide perovskite (N-MEDA)$[PbBr_{4-x}Cl_x]$ (x = 0–1.2) in order to adjust the emission color. They obtained CIE color coordinates of 0.31/0.36 with a QY of a mere 0.5%. Following the work of Dohner, several groups worked 2D layered perovskite to synthesize (i) $(DMEN)PbBr_4$, where DMEN is 2-(dimethylamino)ethylamine, (ii) $(DMAPA)PbBr_4$, where DMAPA is 3-(dimethylamino)-1-propylamine, and (iii) $(DMABA)PbBr_4$, where DMABA is 4-dimethylaminobutylamine (iv) $(EA)_4Pb_3Br_{10-x}Cl_x$ (EA: ethyl ammonium, x = 0, 2, 4, 6, 8, 9.5, and 10) and (v) $(CyBMA)PbBr_4$ based on the highly flexible cis-1,3- bis(methylamino hydrobromide)cyclohexane (CyBMABr) cation.[13] These layered perovskites showed fairly good CIE coordinates, but their QY did not cross even 5%. Apart from this, other conjugate system includes white light emission from $CsPb(Br/I)_3$@anthracene composites were synthesized where anthracene works as a blue emitting component. This composite showed the PLQY of 41.9%.

1.2 Development of double perovskites: Way to overcome issues related to lead-based perovskite

Extensive applications of perovskite materials are found in the realms beyond photovoltaics such as photodetection and light emission. These materials have remarkable properties which lead to observing impressive performance. A perovskite-based solar cell is still far from commercial availability due to severe issues related to toxicity, poor stability to heat, oxygen, moisture, electric

field, and light. Pb^{2+} tends to readily dissolve in water (for instance, rainwater) to form a toxic solution not only capable enough to cause environmental pollution but also harmful to human beings and the ecosystem. Attempts have been made to replace the lead from B site in perovskite ABX_3 crystal structure.

The group IV elements, tin (Sn) and germanium (Ge) have been employed as the replacements for Pb.[14] However, the device performance through this approach has fallen short of the Pb-based ones. For instance, the PCEs reported for Sn-based perovskite solar cells are usually less than 10%.[15] Besides, the easy oxidation of Sn and Ge from the +2 state to the +4 state due to their high energy 5s and 4s orbitals makes them less promising for application in stable and long-term PSCs. Hence it is required to develop a new class of materials which can solve the issues of toxicity and stability retaining the properties and the performance of lead-based perovskite materials.

Recent theoretical calculations validate that a halide double perovskite structure, $A_2B'B''X_6$, which could be formed through a replacement of two toxic Pb^{2+} in the crystal lattice with a monovalent and trivalent metal cations, is a promising alternative.

1.2.1 Crystal Structure

The crystal unit of double perovskite is similar to that of the simple perovskite with only difference in the alternating arrangement of B-site cations in the octahedral cavity as shown in Figure . An ideal halide double perovskite is a network of corner-sharing octahedral with an A-site species occupying the cuboctahedral cavity. The B-site cations occupy the octahedral cavity created by their sixfold coordination with the halide ions.

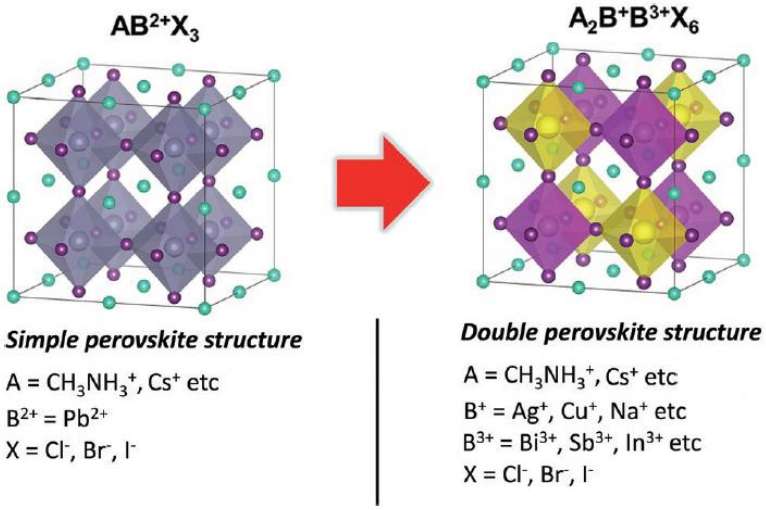

Figure 2: Schematic representation of the structures of simple and double perovskites showing the difference in the elemental composition in the B site. (figure reproduced from Ref.16)[16]

1.2.2 Properties

Transitioning from conventional perovskite structure to double perovskite structure, it is vital to retain or mimic the electronic band composition of perovskites. It should possess shallow defect states, strong absorption and long carrier lifetime. Moreover, it should be stable enough to avoid decomposition, unlike $MAPbI_3$. For lead halide perovskites, the Pb^{2+} has electronic configuration of $6s^2\ 6p^0$. Apart from Pb^{2+}, Tl^+ and Bi^{3+} exhibit such electronic configuration. However, utilizing Tl^+ will not solve the concern as it is toxic. There are reports of using Ag^+ at B site.[17] Although Ag^+ is toxic, poor solubility constant makes it less hazardous. Regardless of mimicking the similar electronic configuration, silver-bismuth based double perovskite shows sub-standard properties such as wide indirect band gap and lower charge carrier transport which subsequently leads to poor PV performance.

1.3 Current Work

Lead halide perovskite NCs have gained considerable attention in the field of optoelectronics and efforts have been made by various research groups to utilize these materials for white light emitting devices. Tunability of emission wavelength is possible via mixed halide composition, but due to the occurrence of anion exchange, the results of these mixed halide components are often compromised. No reports are found that utilizes perovskite NCs as donor/acceptor for white light emission which is stable for a long period in ambient conditions. In this work, Mn-doped $CsPbCl_3$ and Carbon Polymer Dot (CPD) are utilized to form a stable composite for white light emission in ambient condition.

Halide double perovskites exhibit bandgap tunability due to the flexibility in the variation of their chemical components. Since substituting a metal cation to an extent can create a dramatic change in the bandgap of halide double perovskite, this work is based on similar phenomena. Theoretical studies have shown that $Cs_2AgSbCl_6$ has an approximate indirect bandgap of 2.5 eV whereas $Cs_2CuSbCl_6$ has an indirect bandgap of 1.90eVas shown in Figure 3. In this work, a successful attempt was made to synthesize these halide double perovskites and tune the band gap from 1.90eV to 2.5 eV.

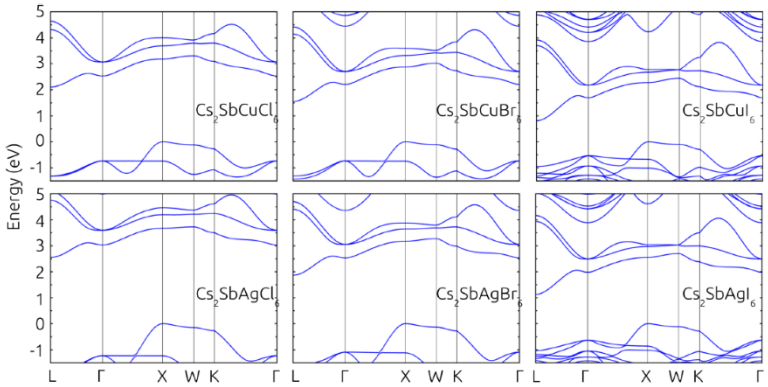

Figure 3: Electronic band structure of antimony-based double perovskites calculated (figure reproduced from Ref.18)[18]

Chapter 2

Experimental Methods

2.1 Materials:

Cesium carbonate (Cs_2CO_3,Sigma Aldrich, 99.995%), lead (II) chloride ($PbCl_2$, Alfa Aesar, 99%), manganese chloride tetrahydrate ($MnCl_2.4H_2O$,Merck,99%), oleylamine (OAm, Sigma Aldrich, 70%), oleic acid (OA, Sigma Aldrich, 90%), 1-octadecene (ODE, Sigma Aldrich, 90%), Trioctyl phosphine(TOP, Sigma Aldrich), Acetone (Rankem, 99%), Dichloro methane (DCM,Rankem,99%) , Methoxy ethanol(Loba Chemie, 99%), Methoxy acetic acid (Alfa Aesar, 97%) and branched polyethylenimine PEI (MWt = 1800) (Alfa Aesar 99%), Methanol (Fischer Scientific, 99%). Antimony Trichloride ($SbCl_3$, SRL, 99%), Copper (I) chloride (CuCl, Sigma Aldrich, >90%), Silver Chloride (AgCl, Sigma Aldrich, 99%), Cesium Chloride (CsCl, Sigma Aldrich, 99.9%), Antimony (III) acetate ($Sb(ac)_3$, Sigma Aldrich , 99%), Diphenyl Ether (DPE,Spectrochem) and Benzoyl Chloride (Bz-Cl, Fishcer Scientific)

2.2 Synthetic Protocol of white light emitting solution

2.2.1 Synthesis of Carbon Polymer Dots:

The procedure reported by Mishra et al.[19]was slightly modified. 1.05 g branched PEI (MW = 1800), and 2.25 g 2-methoxy acetic acid were homogeneously mixed in 20 g 2-methoxy ethanol under stirring (15 min), while the transparent solution turned to straw yellow. Finally, this mixture was heated for 10 min on a pre-heated mantle (at 200^0C) which resulted in the formation of a black solution containing CPDs. Purification of these as-prepared CPDs was done by column chromatography using SiO_2 (60-120 nm) gel as the stationary phase and DCM/methanol (98: 2 w/w) mixture as the mobile phase. Initially, for the preparation of slurry, crude CPD solution was diluted for which 10gm of DCM was used. 3g Silica was then added to dilute CPD solution to form a homogenous slurry followed by drying of DCM. Hence prepared slurry was loaded in small column (with smaller radius). The column was initially eluted with 100% DCM followed by addition of 2% w/w methanol. The column was run until the eluent obtained was cyan (Under UV light Illumination as shown in a digital image). After that, the DCM/methanol mixture was removed from the system via evaporation in a rotary evaporator and 6 ml DCM was added.

2.2.2 Synthesis of Cs-oleate:

The procedure reported by Protesescu et al. was followed.[10] Cs_2CO_3 (0.407g, Aldrich, 99.9%) was loaded into 100 mL 3-neck flask along with ODE (20mL, Sigma-Aldrich, 90%) and oleic acid

(1.25 mL, OA, Sigma-Aldrich, 90%), dried for 1h at 120^0C, and then heated under N_2 to $150^/$C until all Cs_2CO_3 reacted with OA. Since Cs-oleate precipitates out of ODE at room-temperature, it has to be pre-heated to 120^0C before injection.

2.2.3 Synthesis of Mn-Doped $CsPbCl_3$:

The procedure reported by Parobek et al.[20] was slightly modified.$PbCl_2$ (0.1112g), $MnCl_2.(H_2O)_4$ (19.79 mg) (for 25% doped), ODE (7 mL) were added to a 100-mL three neck round bottom flask and were vacuum dried for 1 hr at 120^0C, and then the temperature was raised to 150^0C, and N_2 atmosphere was provided. Dried OAm (0.5 mL) and dried OA (0.5 mL) were subsequently injected.1 ml of TOP was added to the three neck round bottom flask. The temperature was then increased to 180^0C. 1 ml (3-AminoPropyl)Trimethoxy Silane was added to the reaction mixture, and it was allowed to react for 10mins. Cs-oleate (0.4 mL) was then swiftly injected, and the solution was cooled after 10 seconds with an ice bath. The NCs were precipitated with acetone and the centrifuged followed by dissolving in 5 ml of DCM.

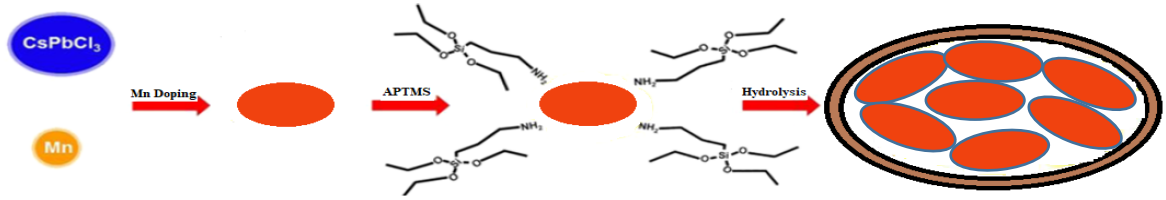

Figure 4: Synthetic protocol of Mn-doped $CsPbCl_3$

2.2.4 Preparation of white light solution:

Mn-doped $CsPbCl_3$ was diluted by adding 0.5ml of it into 9.5ml of DCM. CPD solution was diluted by adding 1 ml of it into 9 ml of DCM. Now, 5 ml Mn-doped perovskite was taken in a vial and 20µL of diluted CPD solution was added to it. After each addition of 20µL Dil. CPD, the mixture solution was vigorously stirred. This addition is carried out until the white light emitting (Under UV, 365nm) solution is obtained.

2.3 Synthetic protocol of double perovskite

2.3.1 Synthesis of double perovskite via solvent synthesis:

For $Cs_2AgSbCl_6$, $SbCl_3$ (228.1mg) and AgCl (143.3mg) was stirred in 5 ml conc. HCl for 30 mins. CsCl was added to the reaction mixture to form a precipitate, and it was allowed to heat at 75^0C for 1 hr. For $Cs_2CuSbCl_6$, CuCl (99mg) was used instead of AgCl. For intermediate $Cs_2Ag_xCu_{1-x}SbCl_6$ (x= 0.25, 0.5, 0.75), stoichiometric amount of Ag and Cu precursor were used.

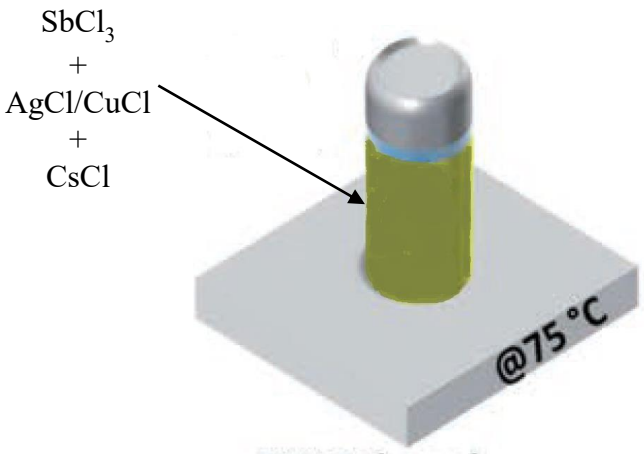

Figure 5: Synthetic protocol of antimony based double perovskite

2.3.2 Synthesis of $Cs_2CuSbCl_6$ via hot injection route:

The synthetic protocol was slightly modified as reported by Manna et al.[21] $Sb(ac)_3$ (0.25mmol), CuCl (0.24mmol), 0.5ml of OAm, 0.5ml of OA, 200 µL of Bz-Cl and 4 ml of DPE were loaded in a three-neck flask and dried under vacuum for 30min at 40^0C. Subsequently, the system was flushed under N_2 and temperature was increased to 105^0C and allowed the reaction mixture to stir at the same temperature for 45min. 0.4ml of Cs-oleate solution was quickly injected to the flask. The reaction was quenched after 5 s by cooling with an ice−water bath. The product solution was added to 7ml ethanol and centrifuged at 4500 rpm for 10 min, the supernatant was discarded, and precipitated NCs were redispersed in 3 mL of toluene.

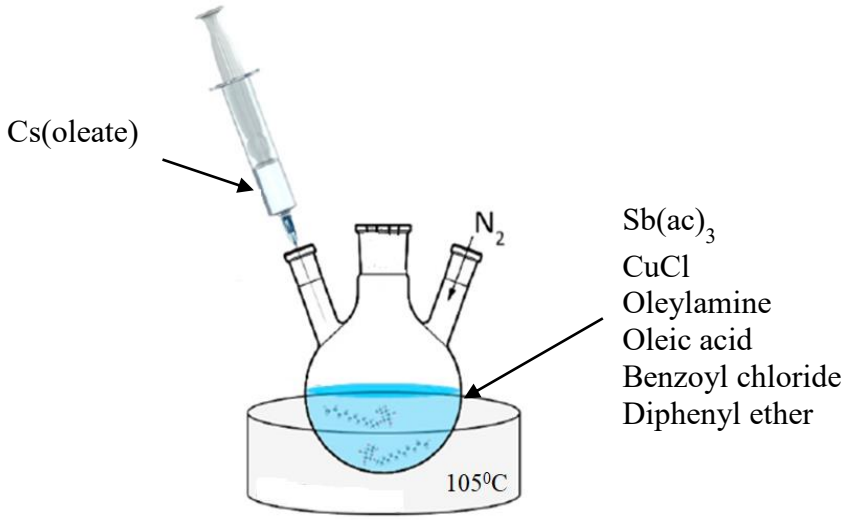

Figure 6: Hot injection route of $Cs_2CuSbCl_6$ synthesis

2.4 Instrumentation:

All steady-state fluorescence experiments were carried out on a Fluoromax-4 (Horiba Jobin Yvon, Edison, NJ). The measurements were made at 25 °C. Following parameters were adjusted for collecting emission spectra: λ_{ex} = 365 nm and λ_{em} (scan range) = 380–700 nm with the integration time of 0.3 s. Time-Correlated Single Photon Counting was carried out on Horiba Fluorohub-B with excitation source of 374 nm. 1% ludox solution was used to record the instrument response function. FTIR (ATR) spectra of the samples were measured in the 4000−400 cm^{-1} range on an Alpha Bruker spectrometer. Powder XRD was carried out on a Rigaku Ultima IV from 10^0 to 70^0 2Ɵ value at a scan rate of 2^0/min. UV- Vis absorption of the samples were measured in 600-300nm range on a Lab India UV 3000 with a slow scan rate at 1nm/sec. TEM images were recorded on Jeol JEM 2100. For double perovskite powder samples, the absorption was recorded via diffuse reflectance mode in Cary 5000 UV-Vis NIR (Agilent Technologies) spectrophotometer at the scan rate of 1 nm/s.

Chapter 3

Results and Discussion

The choice of the starting materials utilized in this white light emitting solution plays an essential role in the stability for an extended period under ambient conditions as these materials are itself stable, unlike most hybrid organic-inorganic system. However, for the characterizations like UV-Vis absorption and fluorescence spectroscopy, Mn-doped $CsPbCl_3$ were transferred to dried toluene.

For the synthesis of the Carbon Polymer Dot (CPD) solution, the organic part, the procedure followed is slightly modified from the as reported procedure by Mishra et al. It is known that when an alkylamine and carboxylic acid are allowed to react at high temperatures (<=200^{0}C), they form Carbon Polymer Dots in the initial stage.[22–24]

To understand what is happening in this system, characterizations were performed by XRD, UV-visible, PL, TCSPC spectroscopy, and TEM analysis.

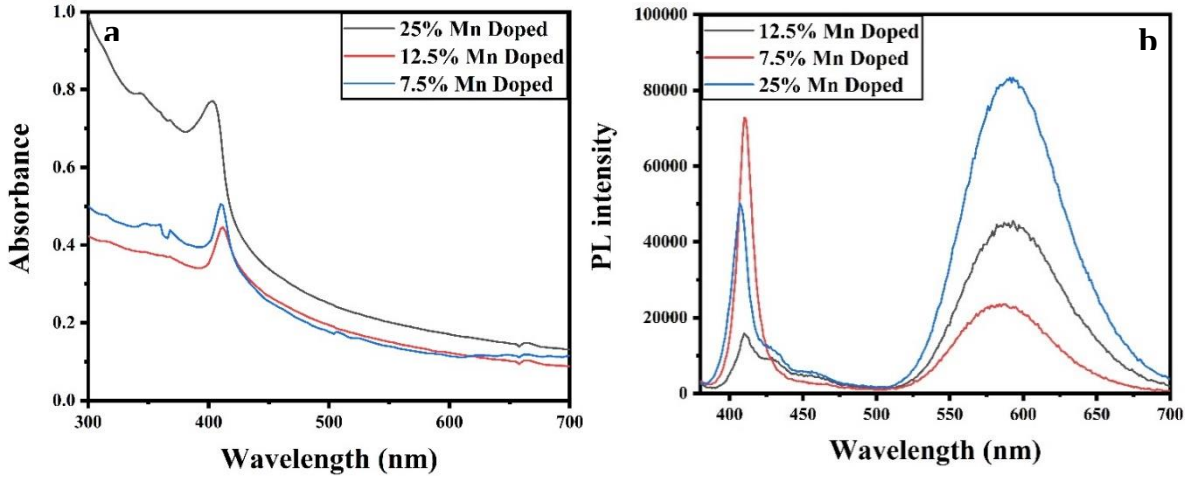

Figure 7: (a) UV-vis and (b) PL spectral study of $CsPbCl_3$ at three different concentrations of Mn^{2+} doping

PL spectra as shown in figure 7 (b) of the as-prepared Mn-doped $CsPbCl_3$ NCs were investigated. For the undoped $CsPbCl_3$ sample, a typical semiconductor exciton emission band centered at 413 nm with a narrow FWHM of 12 nm is detected; for the Mn-doped $CsPbCl_3$ samples, in addition to exciton emission, a broad emission band located at about 600 nm with a FWHM of 70 nm assigned to Mn^{2+}: $^4T_1$ - $^6A_1$ transition is observed. This result further confirms that Mn^{2+} ions are successfully incorporated into $CsPbCl_3$ NCs. With the increase of Mn doping content, a slight redshift of Mn^{2+} emission is found, which can be associated with the lattice contraction induced modification of Mn^{2+} ligand-field.[25]

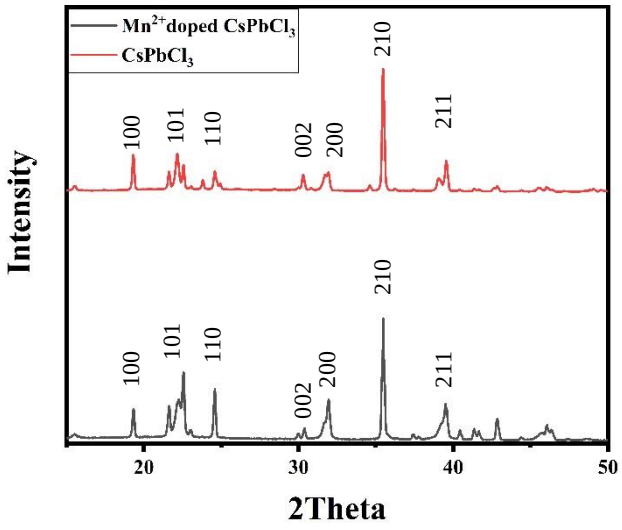

Figure 8: XRD pattern of $CsPbCl_3$ and Mn^{2+}:$CsPbCl_3$

XRD pattern of 25% Mn-doped $CsPbCl_3$ (Figure 8) reveals peak shifts by 0.02^0 to 35.48 from the undoped counterpart. Similarly, for doped perovskite, the peak is observed at 31.94, 19.34 whereas it is at 31.92, 19.32 in undoped counterpart. This shifting towards higher angles with doping is probably ascribed to the gradual substitution of Pb^{2+} (r= 0.133nm, CN= 6) by Mn^{2+} (r = 0.097nm, CN= 6) with smaller ionic radius.[26,27]

TEM images of Mn-doped $CsPbCl_3$ NCs (Figure 9) reveals that these are approximately 20nm cubes. SAED pattern and HRTEM image show the crystalline nature of Mn-doped $CsPbCl_3$.

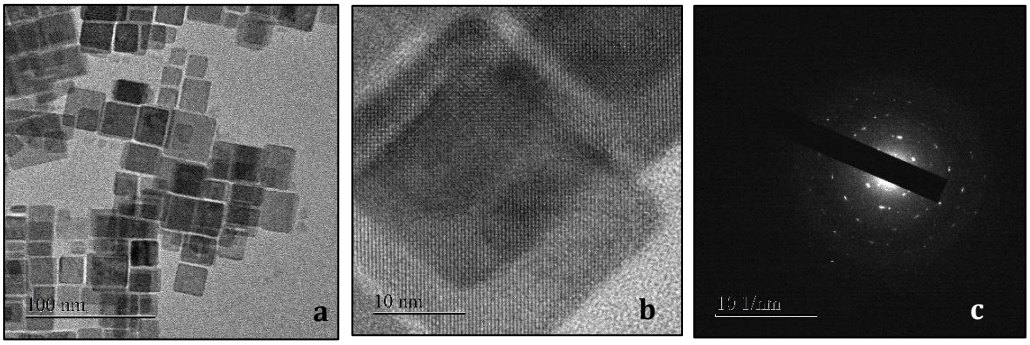

Figure 9. TEM images of Mn^{2+}-$CsPbCl_3$ (a) bright field image shows the existence of cubic shaped Mn-doped $CsPbCl_3$ NCs, (b) lattice fringes corresponding to (210) plane of Mn-doped $CsPbCl_3$ can be seen from the HRTEM image, (c) SAED pattern further proves the crystalline nature of Mn-doped $CsPbCl_3$.

In figure 10, UV-visible absorption shows sharp absorption peaks corresponding to the π - π * transitions, respectively.[28] PL spectra of CPD was recorded. For the fraction utilized of CPD for the white light emitting solution, emission peak centered at 460nm with a broad FWHM of 86 nm.

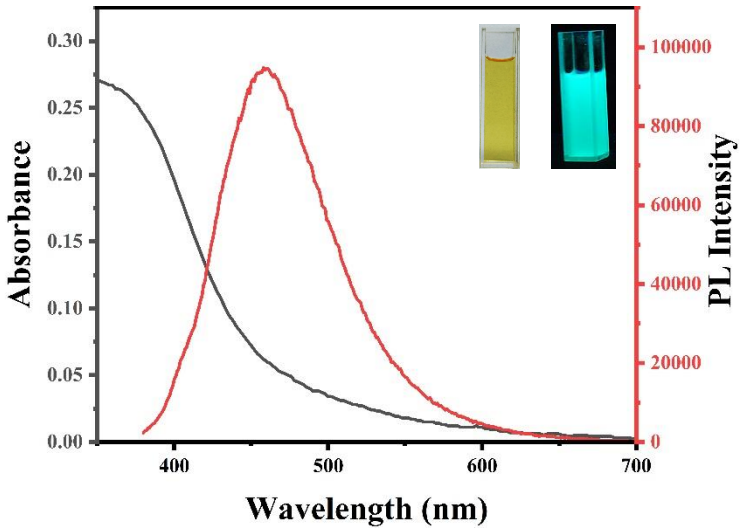

Figure 10. UV-visible and PL spectra of CPD, digital photos of CPD in daylight and UV light

White light emitting solution:

CPD solution was mixed with Mn-doped $CsPbCl_3$ NCs in a stepwise manner to produce white light emission, and the subsequent change in the PL emission was monitored. Progression of PL spectra shows that with a gradual increase in CPD concentration, the PL intensity (peak at 595 nm) of Mn-doped $CsPbCl_3$ NCs started decreasing and simultaneously, increase in the PL intensity of CPD was observed. The change in PL intensity shows the existence of electron[29]/energy[30] transfer between Mn-doped $CsPbCl_3$ and CPD. One can say that the addition of Carbon Polymer Dots leads to the successive

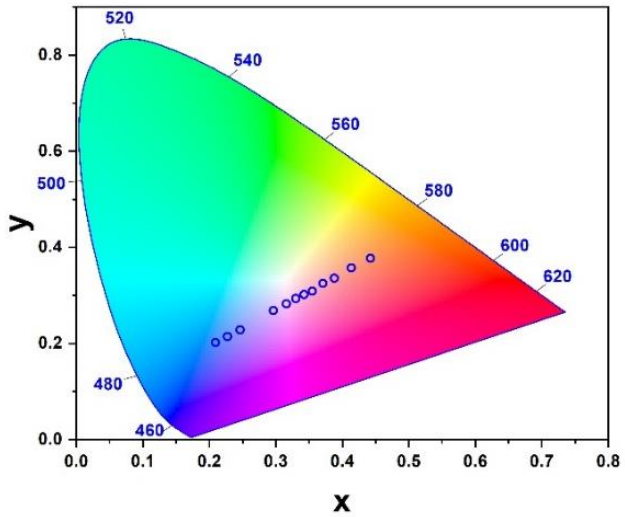

Figure 11. Chromaticity diagram

PL quenching of Mn-doped $CsPbCl_3$, indicating the return of some excited donor NCs to their ground states without emitting photons. After the addition of 200 µL CPD solution, pure white light emission was generated. It covered the full visible spectrum (400-700 nm), and hence it was quite

natural to observe this white light emission. The CIE diagram (Figure 11) with chromaticity color coordinates of (0.30, 0.33) was observed for this white PL emission in solution.

To confirm the morphology and distribution of Mn-doped $CsPbCl_3$ and CPD, we also characterized the white light emitting solution by TEM, and figure 6 shows that CPD is lying on the surface of Mn-doped $CsPbCl_3$ NCs.

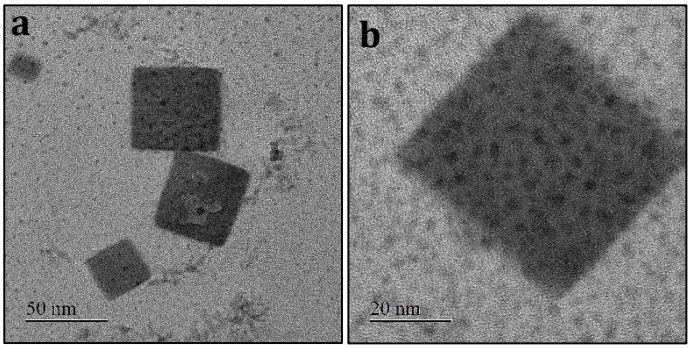

Figure 12. TEM of white light emitting solution (a and b) showing the existence of CPDs on $CsPbCl_3$ NCs.

TCSPC was done to understand the donor-acceptor interactions between Mn-doped $CsPbCl_3$ and CPDs. Reduction in the decay lifetime of the donor molecule is highly probable when two fluorescent molecules interact with each other as donor and acceptor pairs. Hence we monitored the interaction of Mn-doped $CsPbCl_3$ with CPD at the maximum emission wavelength of Mn-doped $CsPbCl_3$ (595nm). There was a continuous decrease in the decay time of Mn^{2+} luminescence after successive addition of CPD solution.

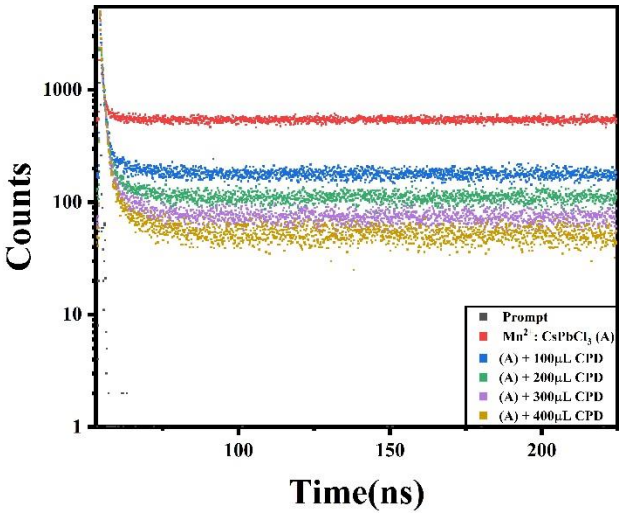

Figure 13. Time-resolved PL of Mn-doped $CsPbCl_3$ and white light composite

Since energy transfer cannot happen through low band gap to high band gap material, the electron transfer process is more favorable as it depends on absolute energy of the valence and conduction band rather than the band gap of the material. Moreover, UV- Vis absorption maxima of CPD is at the lower wavelength (360nm) compared to absorption maxima of Mn-doped $CsPbCl_3$

(404nm) indicate the higher energy of band gap of CPD than Mn-doped $CsPbCl_3$ NCs. Therefore, Energy transfer from Mn-doped $CsPbCl_3$ NCs to CPD is not possible.

The polycrystalline antimony−silver and antimony−copper based double perovskite, $Cs_2AgSbCl_6$ and $Cs_2CuSbCl_6$ were synthesized via solvent synthesis. Figure 14 shows the FESEM image for the $Cs_2AgSbCl_6$. The FESEM images confirm that the product formed is composed of multifaceted polycrystals of 5.6 microns.

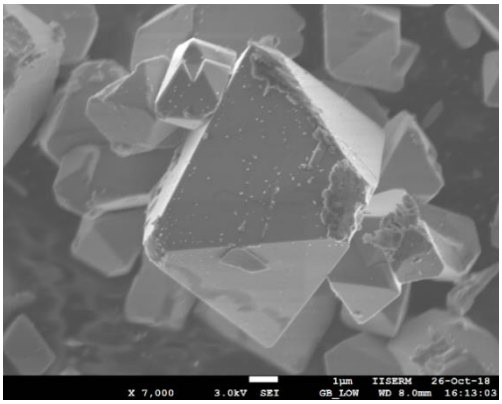

Figure 14: FESEM image of $Cs_2AgSbCl_6$

The PXRD pattern (Figure 15 (a)) of $Cs_2AgSbCl_6$, which matches earlier reports[31], indicates a face-centered cubic double perovskite structure ($Fm\bar{3}m$ space group). Closer examination of the PXRD patterns indicates trace quantities of AgCl in the parent material. The PXRD pattern of $Cs_2CuSbCl_6$ contains the peaks associated with face-centered cubic double perovskite structure along with a few impurity peaks (marked with*).

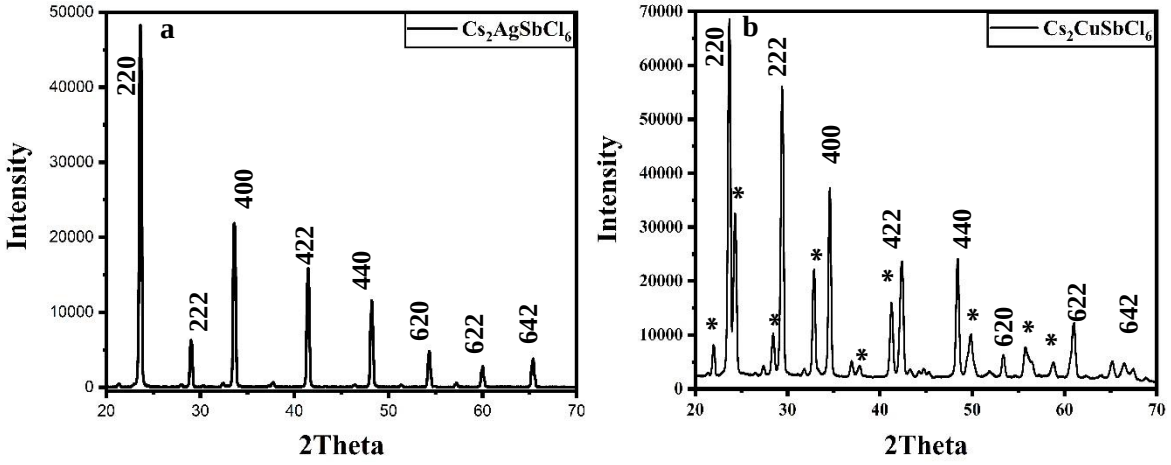

Figure 15. (a) PXRD pattern of $Cs_2AgSbCl_6$ (b) PXRD pattern of $Cs_2AgSbCl_6$

The intermediate $Cs_2Ag_xCu_{1-x}SbCl_6$ (x = 0.25, 0.5, 0.75) was synthesized in similar manner by stoichiometric addition of respective precursors. The percentage of elements (Ag and Cu) that have been incorporated in the product can be calculated through ICP-MS.

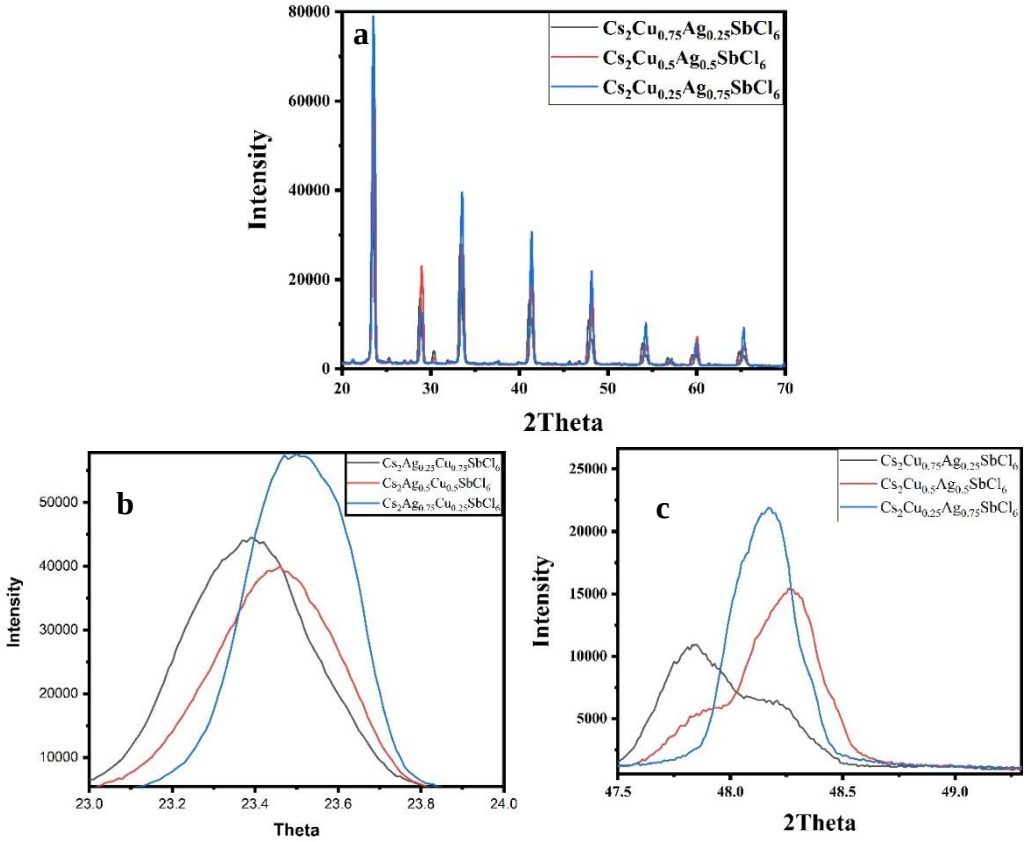

Figure 16. (a) PXRD pattern of intermediate $Cs_2Ag_xCu_{1-x}SbCl$ (x = 0.25, 0.5, 0.75) (b) Shifting of 220 peak (c) shifting of 440 peak.

PXRD patterns (Figure 16b,c) shows slight shifting in the peaks due to change in lattice parameters which is due to different concentration of Ag and Cu incorporation into the lattice.

The ionic radius for Cu+ (0.77 Å) is significantly less than that for Ag^+ (1.29 Å)[32]; thus, a decrease in the lattice parameter due to the incorporation of Cu+ into the crystal lattice is expected. For example, Figure 3b shows that the highly intense (220) peak in the PXRD pattern shifts slightly toward a higher 2θ value with copper incorporation, suggesting that the average lattice parameters are decreasing for the copper incorporated materials and that the Cu+ ion has been inserted into the lattice.

Similar to other halide double perovskites, $Cs_2AgSbCl_6$ & $Cs_2CuSbCl_6$ belongs to the class of the materials that show an indirect bandgap[17,33] Figure 17 shows the absorbance spectrum of the $Cs_2AgSbCl_6$ and $Cs_2CuSbCl_6$. The Tauc plots (Figure 18(b)) show that Cu^+ at B` site reduces the indirect bandgap from 2.53 eV for $Cs_2AgSbCl_6$ to 1.90 eV for $Cs_2CuSbCl_6$.

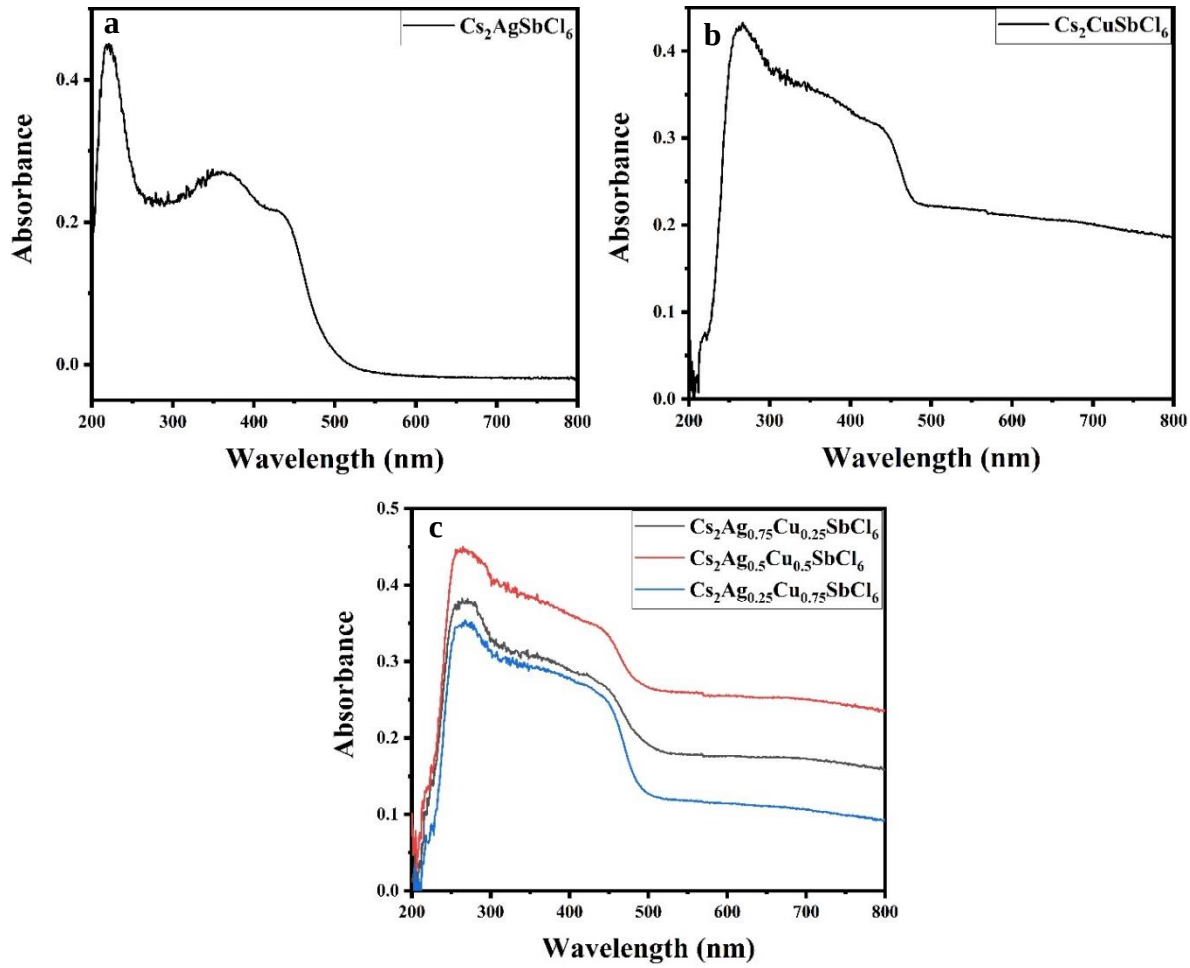

Figure 17. (a) Absorption spectra of $Cs_2AgSbCl_6$ (b) $Cs_2CuSbCl_6$ (c) intermediate $Cs_2Ag_xCu_{1-x}SbCl_6$ (x = 0.25, 0.5, 0.75)

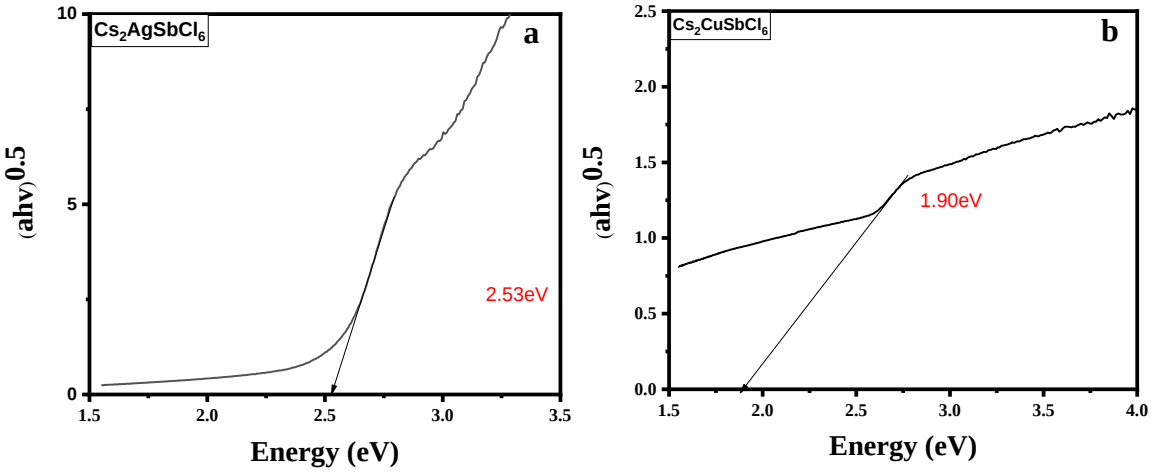

Figure 18. (a) Tauc plot of $Cs_2AgSbCl_6$ (b) $Cs_2CuSbCl_6$

Figure 17c shows the absorption spectrum of intermediate $Cs_2Ag_xCu_{1-x}SbCl_6$ (x = 0.25, 0.5, 0.75). The tauc plot (Figure 19) corresponding to these absorption curves gives us the band gap of 2.03 for x = 0.25, 2.31 for x= 0.5 and 2.40 for x = 0.75. The values of bandgap obtained from these tauc plots show that as the copper concentration increases the band gap dips towards the bandgap of pure $Cs_2CuSbCl_6$ that is 1.90eV.

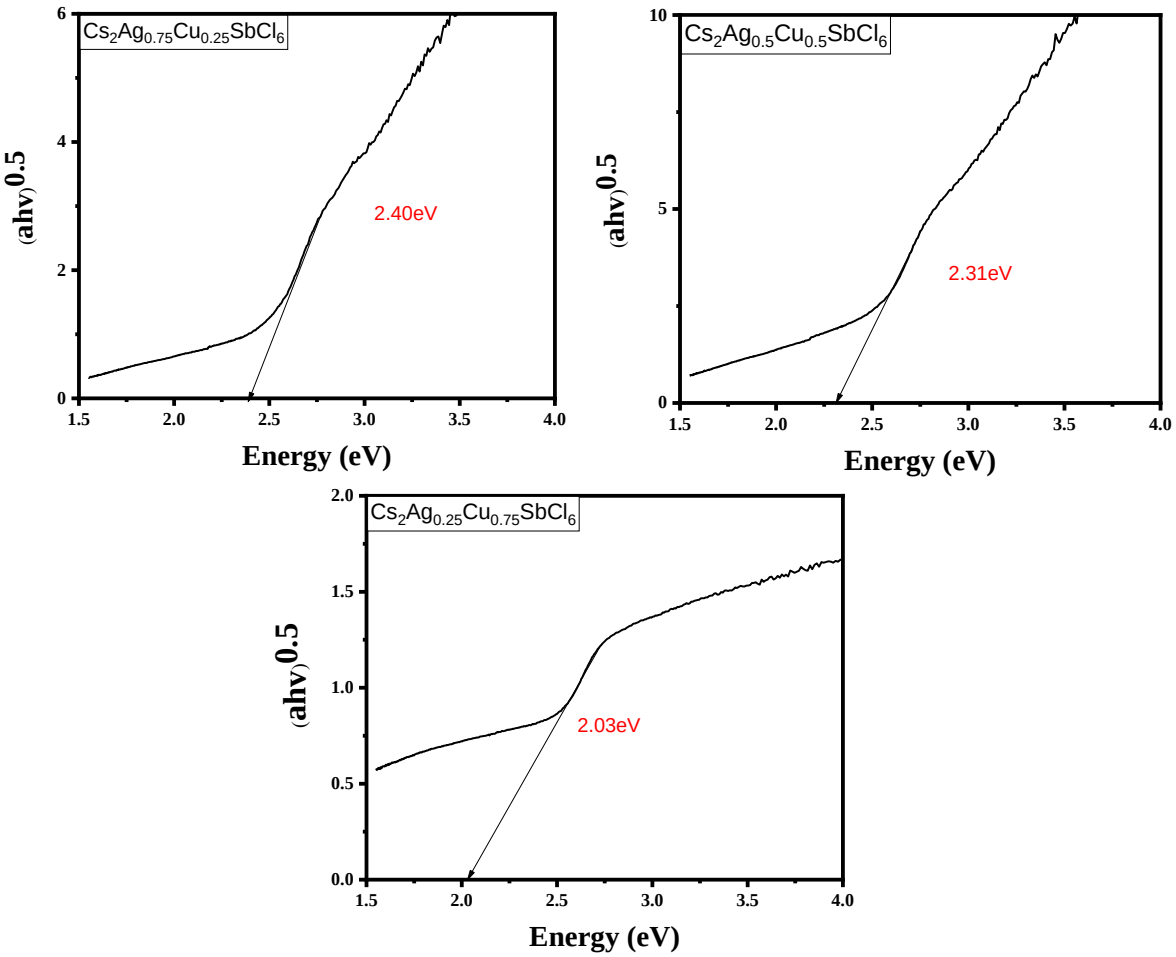

Figure 19. Tauc plot of intermediate $Cs_2Ag_xCu_{1-x}SbCl_6$ (x = 0.25, 0.5, and 0.75)

Figure 20 shows the FESEM image of intermediate $Cs_2Ag_xCu_{1-x}SbCl_6$ (x = 0.25, 0.5, 0.75). Although the morphology of these intermediate is the same as the parent material, the image shows broken faces of the octahedral shaped crystals which have occurred due to the scratching of these materials off the glass vials. Moreover, EDAX analysis was done in the region enclosed in the rectangle of figure 8. The observed atom % is slightly different from the expected atom % as the EDAX analyses over the selected region.

x = 0.75

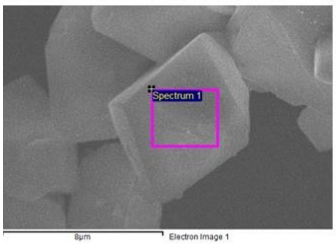

Element	Weight%	Atomic%
Cl K	32.26	62.43
Cu K	0.64	0.70
Ag L	11.73	7.46
Sb L	17.37	9.79
Cs L	38.00	19.62
Totals	100.00	

x = 0.50

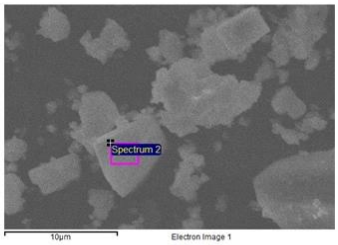

Element	Weight%	Atomic%
Cl K	32.67	63.16
Cu K	0.80	0.86
Ag L	5.40	3.43
Sb L	21.63	12.18
Cs L	39.50	20.37
Totals	100.00	

x = 0.25

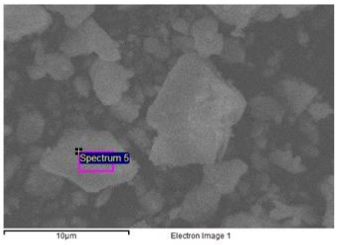

Element	Weight%	Atomic%
Cl K	31.43	61.39
Cu K	1.06	1.15
Ag L	11.16	7.17
Sb L	19.38	11.02
Cs L	36.97	19.26
Totals	100.00	

Figure 20. FESEM images of intermediate $Cs_2Ag_xCu_{1-x}SbCl_6$ (x = 0.25, 0.5, and 0.75) along with elemental composition

The alternative approach of synthesizing $Cs_2CuSbCl_6$ that is, the hot-injection approach was successfully performed. Figure 21 shows the comparison of the XRD pattern of $Cs_2CuSbCl_6$ synthesized via hot injection method with $Cs_2AgSbCl_6$ synthesized via solvent synthesis approach. Further modification in purification might lead to the formation of phase pure $Cs_2CuSbCl_6$.

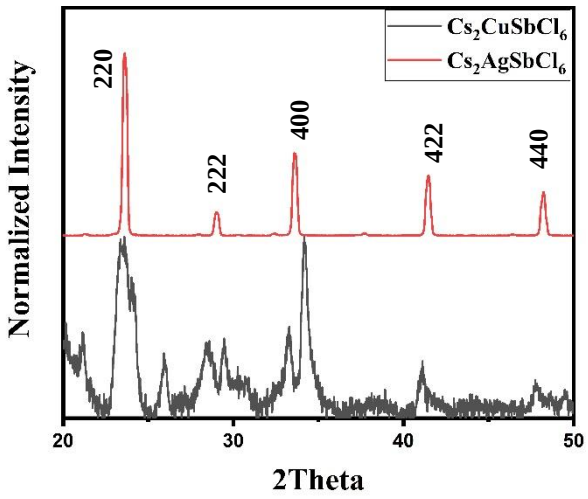

Figure 21: XRD pattern of $Cs_2CuSbCl_6$ synthesized via hot injection method in comparison with $Cs_2AgSbCl_6$ synthesized via solvent synthesis method

Conclusion

A stable solution based white light emitting composite utilizing perovskite. Carbon Polymer Dot is robust and acts as blue emitting species in the composite whereas broad emission corresponding to Mn^{2+} gives red component to this white light emission. In total, Carbon Polymer Dot and Mn-doped $CsPbCl_3$ form a stable white light emitting composite in ambient conditions. The quantum yield of the composite was found out to be 15.5% keeping quinine sulfate as reference. The CIE coordinates obtained from the white light emitting solution is 0.30/0.33.

For the double perovskite work, both the approaches – solvent synthesis and hot injection synthesis, successfully lead to the formation of chloride-based double perovskite system as evident from XRD. Moreover, Tauc plot shows the successful tuning of bandgap done by changing the concentration of Cu and Ag that is from 2.53 eV to 1.9eV.

Future Outlook

Currently, a White light composite made from Mn-doped $CsPbCl_3$ and Carbon Polymer Dots is fabricated in order to utilize it as a white light LED.

For the double perovskite work, bromide and iodide counterpart can be studied to tune the bandgap and subsequently they can act as photovoltaic materials. Moreover, the indirect bandgap can be converted into direct bandgap by doping it with some monovalent or trivalent cation.

Bibliography

(1) Kühn, G. O. Muller, R. Roy. The Major Ternary Structural Families. Crystal Chemistry of Non-Metallic Materials. *Krist. und Tech.* **2007**, *10*, 86.

(2) Köhler, J. Inorganic Solid Fluorides. *Angew.Chem.Int.Ed* **2007**, *99*, 724–725.

(3) Li, C.; Lu, X.; Ding, W.; Feng, L.; Gao, Y.; Guo, Z. Formability of ABX 3 (X = F, Cl, Br, I) Halide Perovskites. *Acta Crystallogr. Sect. B Struct. Sci.* **2008**, *64*, 702–707.

(4) Sarukura, N.; Murakami, H.; Estacio, E.; Ono, S.; El Ouenzerfi, R.; Cadatal, M.; Nishimatsu, T.; Terakubo, N.; Mizuseki, H.; Kawazoe, Y.; et al. Proposed Design Principle of Fluoride-Based Materials for Deep Ultraviolet Light Emitting Devices. *Opt. Mater. (Amst).* **2007**, *30*, 15–17.

(5) Zhang, F.; Mao, Y.; Park, T. J.; Wong, S. S. Green Synthesis and Property Characterization of Single-Crystalline Perovskite Fluoride Nanorods. *Adv. Funct. Mater.* **2008**, *18*, 103–112.

(6) Goldschmidt, V. M. Die Gesetze Der Krystallochemie (The Laws of Cristallochemistry). *Naturwissenschaften* **1926**, *14*, 477–485.

(7) Talapin, D. V.; Lee, J. S.; Kovalenko, M. V.; Shevchenko, E. V. Prospects of Colloidal Nanocrystals for Electronic and Optoelectronic Applications. *Chem. Rev.* **2010**, *110*, 389–458.

(8) Kojima, A.; Teshima, K.; Shirai, Y.; Miyasaka, T. Organometal Halide Perovskites as Visible-Light Sensitizers for Photovoltaic Cells. *J. Am. Chem. Soc.* **2009**, *131*, 6050–6051.

(9) NREL. www.nrel.gov/pv/assets/images/efficiency-chart.png.

(10) Protesescu, L.; Yakunin, S.; Bodnarchuk, M. I.; Krieg, F.; Caputo, R.; Hendon, C. H.; Yang, R. X.; Walsh, A.; Kovalenko, M. V. Nanocrystals of Cesium Lead Halide Perovskites (CsPbX3, X = Cl, Br, and I): Novel Optoelectronic Materials Showing Bright Emission with Wide Color Gamut. *Nano Lett.* **2015**, *15*, 3692–3696.

(11) Kang, J.; Wang, L. W. High Defect Tolerance in Lead Halide Perovskite CsPbBr3. *J. Phys. Chem. Lett.* **2017**, *8*, 489–493.

(12) Dohner, E. R.; Hoke, E. T.; Karunadasa, H. I. Self-Assembly of Broadband White-Light Emitters. *J. Am. Chem. Soc.* **2014**, *136*, 1718–1721.

(13) Bidikoudi, M.; Fresta, E.; Costa, R. D. White Perovskite Based Lighting Devices. *Chem. Commun.* **2018**, *54*, 8150–8169.

(14) Yang, D.; Lv, J.; Zhao, X.; Xu, Q.; Fu, Y.; Zhan, Y.; Zunger, A.; Zhang, L. Functionality-Directed Screening of Pb-Free Hybrid Organic-Inorganic Perovskites with Desired Intrinsic

Photovoltaic Functionalities. *Chem. Mater.* **2017**, *29*, 524–538.

(15) Klug, M. T.; Osherov, A.; Haghighirad, A. A.; Stranks, S. D.; Brown, P. R.; Bai, S.; Wang, J. T. W.; Dang, X.; Bulović, V.; Snaith, H. J.; et al. Tailoring Metal Halide Perovskites through Metal Substitution: Influence on Photovoltaic and Material Properties. *Energy Environ. Sci.* **2017**, *10*, 236–246.

(16) Igbari, F.; Wang, Z. K.; Liao, L. S. Progress of Lead-Free Halide Double Perovskites. *Adv. Energy Mater.* **2019**, *9*, 1803150.

(17) Slavney, A. H.; Hu, T.; Lindenberg, A. M.; Karunadasa, H. I. A Bismuth-Halide Double Perovskite with Long Carrier Recombination Lifetime for Photovoltaic Applications. *J. Am. Chem. Soc.* **2016**, *138*, 2138–2141.

(18) Volonakis, G.; Filip, M. R.; Haghighirad, A. A.; Sakai, N.; Wenger, B.; Snaith, H. J.; Giustino, F. Lead-Free Halide Double Perovskites via Heterovalent Substitution of Noble Metals. *J. Phys. Chem. Lett.* **2016**, *7*, 1254–1259.

(19) Mishra, M. K.; Kundu, S.; De, G. Stable Fluorescent CdS:Cu QDs and Their Hybridization with Carbon Polymer Dots for White Light Emission. *J. Mater. Chem. C* **2016**, *4*, 1665–1674.

(20) Parobek, D.; Roman, B. J.; Dong, Y.; Jin, H.; Lee, E.; Sheldon, M.; Son, D. H. Exciton-to-Dopant Energy Transfer in Mn-Doped Cesium Lead Halide Perovskite Nanocrystals. *Nano Lett.* **2016**, *16*, 7376–7380.

(21) Locardi, F.; Cirignano, M.; Baranov, D.; Dang, Z.; Prato, M.; Drago, F.; Ferretti, M.; Pinchetti, V.; Fanciulli, M.; Brovelli, S.; et al. Colloidal Synthesis of Double Perovskite Cs2AgInCl6 and Mn-Doped Cs2AgInCl6 Nanocrystals. *J. Am. Chem. Soc.* **2018**, *140*, 12989–12995.

(22) Song, Y.; Zhu, S.; Zhang, S.; Fu, Y.; Wang, L.; Zhao, X.; Yang, B. Investigation from Chemical Structure to Photoluminescent Mechanism: A Type of Carbon Dots from the Pyrolysis of Citric Acid and an Amine. *J. Mater. Chem. C* **2015**, *3*, 5976–5984.

(23) Bourlinos, A. B.; Stassinopoulos, A.; Anglos, D.; Zboril, R.; Georgakilas, V.; Giannelis, E. P. Photoluminescent Carbogenic Dots. *Chem. Mater.* **2008**, *20*, 4539–4541.

(24) Dong, Y.; Wang, R.; Li, G.; Chen, C.; Chi, Y.; Chen, G. Polyamine-Functionalized Carbon Quantum Dots as Fluorescent Probes for Selective and Sensitive Detection of Copper Ions. *Anal. Chem.* **2012**, *84*, 6220–6224.

(25) Chen, D.; Fang, G.; Chen, X. Silica-Coated Mn-Doped CsPb(Cl/Br)3 Inorganic Perovskite Quantum Dots: Exciton-to-Mn Energy Transfer and Blue-Excitable Solid-State Lighting. *ACS Appl. Mater. Interfaces* **2017**, *9*, 40477–40487.

(26) Guria, A. K.; Dutta, S. K.; Adhikari, S. Das; Pradhan, N. Doping Mn2+ in Lead Halide

Perovskite Nanocrystals: Successes and Challenges. *ACS Energy Lett.* **2017**, *2*, 1014–1021.

(27) Liu, W.; Lin, Q.; Li, H.; Wu, K.; Robel, I.; Pietryga, J. M.; Klimov, V. I. Mn2+-Doped Lead Halide Perovskite Nanocrystals with Dual-Color Emission Controlled by Halide Content. *J. Am. Chem. Soc.* **2016**, *138*, 14954–14961.

(28) Li, X.; Zhang, S.; Kulinich, S. A.; Liu, Y.; Zeng, H. Engineering Surface States of Carbon Dots to Achieve Controllable Luminescence for Solid-Luminescent Composites and Sensitive Be2+ Detection. *Sci. Rep.* **2014**, *4*, 4976.

(29) Kundu, S.; Sadhu, S.; Bera, R.; Paramanik, B.; Patra, A. Fluorescence Dynamics and Stochastic Model for Electronic Interaction of Graphene Oxide with CdTe QD in Graphene Oxide-CdTe QD Composite. *J. Phys. Chem. C* **2013**, *117*, 23987–23995.

(30) Funston, A. M.; Jasieniak, J. J.; Mulvaney, P. Complete Quenching of CdSe Nanocrystal Photoluminescence by Single Dye Molecules. *Adv. Mater.* **2008**, *20*, 4274–4280.

(31) Deng, W.; Deng, Z. Y.; He, J.; Wang, M.; Chen, Z. X.; Wei, S. H.; Feng, H. J. Synthesis of Cs2AgSbCl6 and Improved Optoelectronic Properties of Cs2AgSbCl6/TiO2 Heterostructure Driven by the Interface Effect for Lead-Free Double Perovskites Solar Cells. *Appl. Phys. Lett.* **2017**, *111*, 151602.

(32) R. D. Shannon. Revised Effective Ionic Radii and Systematic Studies of Interatomic Distances in Halides and Chalcogenides. *Acta Cryst.* **1976**, *A32*, 751–767.

(33) Slavney, A. H.; Leppert, L.; Bartesaghi, D.; Gold-Parker, A.; Toney, M. F.; Savenije, T. J.; Neaton, J. B.; Karunadasa, H. I. Defect-Induced Band-Edge Reconstruction of a Bismuth-Halide Double Perovskite for Visible-Light Absorption. *J. Am. Chem. Soc.* **2017**, *139*, 5015–5018.